Depositional environments and historical contamination as a framework to reconstruct fluvial sedimentary evolution

Sophia Vauclin, Brice Mourier, André-Marie Dendievel, Nicolas Noclin, Hervé Piégay, Philippe Marchand, Anaïs Vénisseau, Anne de Vismes, Irène Lefèvre, Thierry Winiarski

Depositional environments and historical contamination as a framework to reconstruct fluvial sedimentary evolution

Sophia Vauclin[1]*, Brice Mourier[1], André-Marie Dendievel[1], Nicolas Noclin[1], Hervé Piégay[2], Philippe Marchand[3], Anaïs Vénisseau[3], Anne de Vismes[4], Irène Lefèvre[5], & Thierry Winiarski[1]

[1]Univ Lyon, Université Claude Bernard Lyon 1, CNRS, ENTPE, UMR 5023, LEHNA, F-69518, Vaulx-en-Velin, France

[2]Univ Lyon, Université Jean Moulin Lyon 3, CNRS, ENS Lyon, UMR 5600 EVS, F-69342, Lyon Cedex 7, France

[3]ONIRIS, INRAE, LABERCA Route de Gachet-Site de la Chantrerie-CS 50707, Nantes, F-44307, France

[4]LMRE, IRSN, PRP-ENV/STEME/LMRE, F-91400, Orsay, France

[5]LSCE, CEA, UMR8212, F-91198, Gif-sur-Yvette, France

*Corresponding author: sophia.vauclin@developpement-durable.gouv.fr

Abstract:

In this study, we explore the variability of sedimentation conditions (grain-size, accumulation rate, contamination, etc.) according to fluvial depositional environments. Indeed, sediment cores are commonly used as archives of natural and anthropogenic activities in hydrosystems, but their interpretation is often complex, especially in a fluvial context where many factors may affect the quality, continuity, and resolution of the record. It is therefore critical to thoroughly understand the nature and dynamics of an environment in which a sediment core is sampled to be able to interpret it. To that end, four depositional environments from a bypassed reach of the Rhône River were comparatively investigated through geophysical methods in order to assess the range of sedimentation

conditions: a floodplain, a semi-active secondary channel, an active secondary channel, and a dam reservoir. Sediment cores were retrieved from each environment and thoroughly characterized (grain-size, Total Organic Carbon, organic contaminants, etc.). Robust age-depth models were elaborated for each of them based on ^{137}Cs, ^{210}Pb, and Persistent Organic Pollutants (POPs) trends. The results show that each depositional environment recorded a different time-period, and therefore different contamination levels and trends. In particular, a shift from polychlorinated biphenyls (PCBs) to polybrominated diphenyl ethers (PBDEs) as the predominant POP in the sediments can be observed, the tipping point being set in the 1970s. Two types of infrastructure-induced legacy sediments related to two periods of river engineering in the reach were also identified using grain-size analysis. The combination of geophysical methods and sediment cores is therefore confirmed as a relevant methodology that should be promoted in fluvial contexts in order to reconstruct the sedimentary evolution of fluvial corridors. The study also highlights the challenges of dating recent fluvial sediments and proposes a multi-proxy dating methodology using POPs contamination trends.

Keywords: Age-depth model; depositional environment; natural archive; polybrominated diphenyl ethers; polychlorinated biphenyls; sediment core.

1. Introduction

Monitoring the signals -anthropogenic or natural – that sediments record may provide invaluable information to understand the long and short-term evolution of a hydrosystem. Indeed, numerous studies have shown that sediments may be used as archives of meteorological events (e.g. storms: Vliet-Lanoe et al., 2014; Pouzet and Maanan, 2020, floods: Jones et al., 2012; Toonen et al., 2015), historical contamination (e.g. Bigus et al., 2014, Dendievel et al., 2020) or other anthropogenic impacts such as pre-historic gullying (Dotterweich, 2005; Vanwalleghem et al., 2006), agriculture intensification (Brooks and Brierley, 1997; Fuller et al., 2015) or river manipulations (Surian and Rinaldi, 2003; Vauclin et al., 2019). The diversity of anthropogenic disturbances potentially recorded in sediments even led

to the establishment of the term “legacy sediments” to refer to sediments resulting from past or contemporary human activities such as land-use, contamination (Walter and Merritts, 2008; James, 2013; Wohl, 2015) or river engineering (Vauclin et al., 2020). However, in order to use wisely the information contained in sediment deposits, it is critical to understand their recording ability depending on their geographical and geomorphological context. Factors such as connectivity of the environment and sediment accumulation rate, for example, will affect the continuity and precision of the record, while sediment characteristics such as grain-size or organic carbon content will specifically affect contamination chronicles (Karickhoff et al., 1979). Some environments such as lakes allow continuous and regular sedimentation. Sediments deposited in such contexts are therefore reliable and lasting archives that tend to be preferentially used to study local or atmospheric contamination trends, anthropogenic activities in the upstream catchment (Guzzella et al., 2008; Guédron et al., 2016) or long-term climatic or environmental changes (Simonneau et al., 2013; Zolitschka et al., 2013). In contrast, there is usually a large diversity of depositional environments in fluvial contexts (e.g. floodplains, oxbow lakes, secondary channels, paleochannels, weir ponds, groyne fields, locks, etc.). Those environments may have various levels of connectivity and therefore various recording capacities (Dhivert et al., 2015) and temporalities, making the interpretation of sedimentary archives challenging. When implemented, river engineering may also profoundly reshape the natural depositional environments and alter their sedimentation processes. Additionally, sediment accumulation rates in a fluvial context are often dependent on hydrological events: sustained low-water conditions might result in a decreased or non-existent sedimentation, while a flood might bring a dozen centimetres of sediments in the span of a few hours or remobilize previously settled sediments, generating discontinuous archives. The dating of fluvial sediments is therefore key for a relevant interpretation of a sedimentary sequence, but might also prove challenging, as classic methods such as ^{210}Pb or ^{137}Cs might not give satisfying results due to the continuity issues previously mentioned.

In that light, investigating the various fluvial compartments appears as essential for any retrospective approach implemented from fluvial sediments. It is the only way to potentially reconstruct the entire

timeline of a river, where individual sediment sequences are inherently incomplete due to the changing nature of fluvial systems. It might also allow to establish links between sediments and their deposition processes, and identify sediment sequences resulting from changes in fluvial systems. It is especially important as rivers are characterized by complex sedimentary dynamics that are often further segmented by anthropogenic modification of their morphology and functioning. However, when suitably interpreted, sedimentary sequences may allow to reconstruct the evolution of a river corridor in correlation with the anthropogenic pressures it was subject to throughout time. Such an understanding is essential to implement relevant restoration measures and mitigate further anthropogenic impact on the river system (Wohl et al., 2005; Arnaud et al., 2015; Słowik, 2015; Eschbach et al., 2018).

The aims of this study are:

- to highlight the temporal and qualitative variability of fluvial sediment records –especially regarding contaminant chronicles– depending on their depositional environment,
- to use these findings to reconstruct the sedimentary evolution of a large river,
- overall, to propose a robust methodology for the use of fluvial sediment deposits as records of natural or anthropogenic disturbances in an actively changing fluvial system.

To this end, four distinct depositional environments from a 12km-long heavily anthropized reach of the Rhône River (France) are investigated in a comparative approach. Their dynamics and the chronology of their records are assessed and compared through a combination of geophysical surveys

and dated sediment cores in order to describe the diversity of sedimentary records and reconstitute the trajectory of this actively adjusting fluvial area.

2. Material and methods

2.1. Study area

The Rhône River is an 812 km-long river that flows from the Furka Glacier in Switzerland to the Mediterranean Sea in France (Fig. 1.a.). Its catchment covers 98 500 km² -of which 90 500 km² are in France- and its average inter-annual discharge is approximately 1 700 $m^3 s^{-1}$ at the estuary. It has a long history of human influence and the earliest traces of agriculture along the river date back to around 7 500 years ago (Berger et al. 2019). As most major rivers in Europe, the Rhône is highly engineered, with numerous dikes, groynes and 19 dams along its French course. Those infrastructures have impacted the river in many ways: increased transport capacity, reduced sediment load, channel armouring, narrowing and incision, increased slope, increased trapping efficiency, etc. (Petit et al., 1996; Bravard et al., 1999; Arnaud-Fassetta, 2003; Parrot, 2015; Tena et al., 2020).

The study area (known as PDR for « Péage-de-Roussillon ») is located 50 km downstream from the metropolitan city of Lyon (Fig. 1.a). It consists of a 12 km-long reach with a bypass configuration typical of the Rhône River: the historical main channel is closed by an upstream run-of-river dam and bypassed by an artificial canal (Fig. 1.b). The area has undergone two phases of engineering in the last 200 years. River training and flood protection infrastructures were implemented from the mid-19th century to the early 20th century: non-submersible dikes were built on the floodplain, and submersible dikes and groynes were implemented in the river in order to cut secondary arms and straighten the main channel. From 1974 to 1978, the area was heavily modified to produce hydroelectricity: an 11 km-long canal was dug out in parallel to the existing one and equipped with a lock and a power plant, and the historical channel was closed with a run-of-river dam to divert most of the discharge in the canal. As a result, only a minimum instream flow of 50 to 125 m^3/s is maintained nowadays in the bypassed channel (GRAIE, 2016), while the inter-annual discharge upstream of the area is 1080 $m^3 s^{-1}$. The

historical channel is still used to accommodate flood flows that exceed the maximum discharge processed by the hydropower plant (1600 $m^3 s^{-1}$).

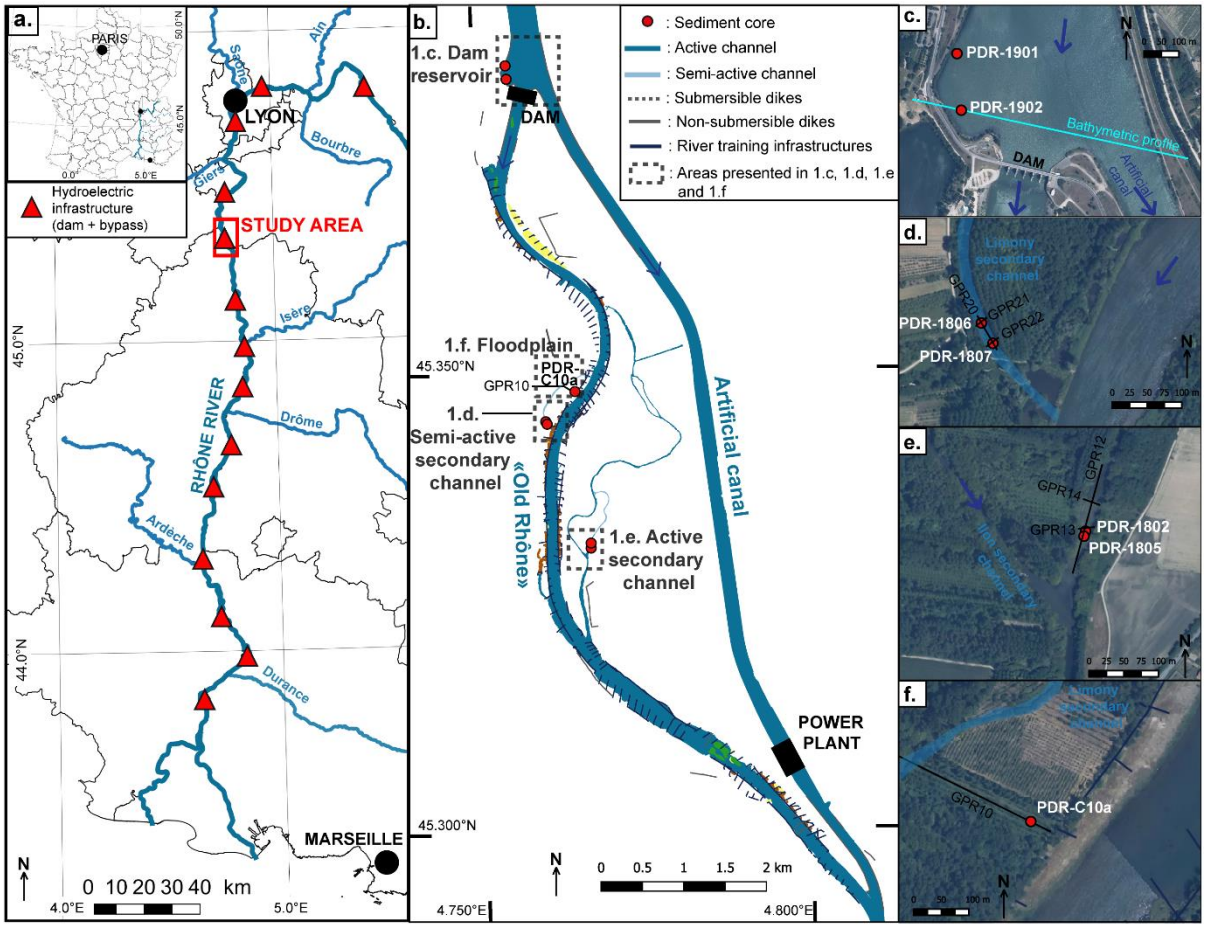

Figure 1: a. Location of the study area along the Rhône River; b. Overview of the study area and its river infrastructures (NB: core PDR-C10a has been previously published in Vauclin et al., 2019); c. Study site: Saint-Pïerre-de-Boeuf dam reservoir; d. Study site: Limony secondary channel; e. Study site: Ilon secondary channel. [IN COLOR]

Inside this area, four fluvial compartments were chosen in an attempt to characterize and compare four distinct types of depositional environments. The selected study sites exhibit different hydro-sedimentary dynamics which have been created or impacted by various periods and types of river engineering, as shown in a planimetric analysis of the area published in Tena et al. (2020).

- The Saint-Pierre-de-Boeuf dam reservoir is a recent compartment as it was built in 1978 upstream of the bypassed section (Fig. 1.b). It is a run-of-river installation, therefore most

sediments flow through the dam, especially during flooding. However, a recess zone along the right bank allows sediment accumulation (Fig. 1.c).

- The Ilon secondary channel (Fig. 1.e) was part of a major arm of the Rhône River until the implementation of river training structures in the 1880s, when it became less connected as both its inflow and outflow were barred by submersible dikes and groynes (Vauclin et al., 2019; Tena et al., 2020). In the 1950s, the Ilon secondary channel had lost in width but both its ends were still linked to a secondary arm of the main stream. Following the bypass implementation in 1978, the upstream entrance got disconnected and the channel is now supplied by its downstream end only but still underwater all year-long. It is further referred to as an active secondary channel.
- The Limony secondary channel (Fig. 1.d) used to be an active arm of the river prior to the first engineering phase. Both its entrance and outflow were then closed by submersible dykes in the 1880s and it quickly became disconnected from the main channel (Vauclin et al., 2019; Tena et al., 2020). Nowadays, it is mostly supplied by groundwater and flooded by the river several times a year. It is further referred to as a semi-active secondary channel.
- An overbank floodplain location that used to be flooded regularly prior to the bypass implementation but is entirely disconnected from the river since the 1980s (Vauclin et al., 2019). Note that part of the results from this site have already been published (Vauclin et al., 2019; Vauclin et al., 2020) but are used in this study for a broader comparison of different depositional environments.

2.2. Bathymetric and geophysical analysis

Bathymetric surveys measured along a transect from the Saint-Pierre-de-Boeuf dam reservoir on which a sediment core is located (Fig. 1.c) were provided by the CNR (Compagnie Nationale du Rhône; company in charge of the river management). They were available for six dates: 1980, 1999, 2004, 2008, 2012 and 2018, and allowed to reconstruct the progressive filling of the reservoir with sediments.

159 Ground Penetrating Radar (GPR) is a non-invasive geophysical method used to obtain a high-resolution
160 image of shallow subsurface structures (Davis and Annan, 1989). It is based on the generation and
161 propagation of discrete pulses of high frequency (MHz) electromagnetic energy through the
162 sediments. It allows the assessment of subsurface spatial structures up to a depth of 10–20 m over
163 extended areas (Huggenberger et al., 1994; Beres et al., 1999) with a resolution ranging between 10
164 cm and 1 m (Jol, 1995). It can be used on the ground (GPR) or on shallow water bodies (1 to 2 meters
165 of water depth) where it is then referred to as Water Ground Penetrating Radar (WGPR: Annan et
166 Davis, 1977).

167 A 500 m-long GPR survey (GPR10) was acquired on the floodplain site in 2016. Three GPR profiles were
168 acquired on the active secondary channel (GPR12, GPR13, and GPR14; 160 m, 22 m, and 25 m
169 respectively; only) in October 2018 (Fig. 1.e). The GPR was used in WGPR configuration from a small
170 boat as there was a water depth of 60 to 70 cm in the channel at the time. Three GPR profiles were
171 acquired on the semi-active secondary channel (GPR20, GPR21, and GPR22; 55 m, 18 m, and 20 m
172 respectively) in October 2018 as well (Fig. 1.d). The measurements were made directly on the ground
173 as there was no water in the channel at the time. On the floodplain, one 500 m-long survey was
174 acquired in 2016 (GPR10). All GPR surveys were carried out with the GSSI SIR 3000 system (Geophysical
175 Survey System Inc., Salem, USA), operated with a shielded antenna at a central frequency of 400 MHz,
176 running in monostatic mode. In addition, a topographic survey using a GPS Trimble station was
177 performed to localize the surveys. Velocities of 0.11 m ns^{-1} (measured by a common mid-point
178 procedure) and 0.076 m ns^{-1} (from Lin et al., 2009) were used for the terrestrial and aquatic surveys
179 respectively, in order to calibrate the profile depths. The data processing was performed using the GSSI
180 Radan 7 software.

2.3. Sediment characteristics

2.3.1. Core sampling

The core sampling locations were chosen after a quick on-site analysis of the geophysical surveys so that the cores would cross interesting sedimentary structures. Two underwater cores (PDR-1901 and PDR-1902) of 72 and 104 cm respectively were retrieved from the dam reservoir in July 2019 with an UWITEC® corer (Uwitec, Mondsee, Austria) fitted with a 2 m-long and 90 mm-diameter plastic liner. Two underwater cores (PDR-1802 and PDR-1805) of 94 and 57 cm respectively were sampled from a small boat in the active secondary channel (Fig. 1.e) in October 2018 with the same corer. Three terrestrial cores (PDR-1806a, PDR-1806b and PDR-1807) of 82, 74.5 and 78.6 cm respectively were retrieved from the Limony secondary channel in dewatered state with a Cobra TT percussion driller in October 2018. Cores PDR-1806b was drilled 1 m apart from PDR-1806a in a 60 cm-deep pit, in order to combine the two cores; the resulting mastercore (PDR-1806) is 108 cm-long. A 111 cm-long core (PDR-C10a) was sampled from the floodplain site in 2016 with the same Cobra TT percussion driller. The detailed characteristics of the studied sediment cores are summarized in Table S1.

2.3.2. Grain-size characteristics

Grain-size was measured on all cores every 0.5 to 1 cm with a Mastersizer 2000© (Malvern Panalytical) particle size analyzer mounted with a hydro SM small volume dispersion unit. Descriptive grain-size statistics (D50, mode, D10, D90, skewness, etc.) were computed with the Gradistat software (Blott and Pye, 2001). To represent the grain-size distributions (GSD) as extensively as possible, heatmaps of each core were plotted; for each measured sample, the percentage of each grain-size class is represented by a colour scale. Unmixing of the sets of grain-size distributions was carried out on all sediment cores simultaneously through end-member modelling analysis (EMMA) with the R package EMMAgeo (Dietze et al., 2012). EMMA is a compositional method based on the assumption that any GSD is a mixture of sediment populations corresponding to different mechanisms of production and/or transport (Weltje and Prins, 2003; Toonen et al., 2015; Dietze et al., 2016). A linear mixing model is therefore applied to an array of GSDs and allows to identify meaningful end-members that correspond

to the most representative populations of the GSDs (Weltje and Prins, 2007). The end-member scores (percentage of representation of the different end-members) were plotted as a function of the depth for each core.

2.3.3. Geochemical and contaminants analyses

Rock-eval pyrolysis was used to analyze several organic carbon-associated parameters of the sediments, such as the total organic carbon (TOC). The analyses were carried out at the ISTO laboratory (Orléans, France) with a 4 cm step on cores PDR-C10a, PDR-1802, PDR-1806, and PDR-1902.

Polychlorinated biphenyls (PCBs) and polybrominated diphenyl ethers (PBDEs) were analyzed. PCBs were chosen as they are well-studied POPs whose temporal trends are reasonably well-known in the Rhône River (e.g. Desmet et al., 2012, Mourier et al., 2014, Dendievel et al., 2020). Meanwhile, PBDEs are emerging POPs that have been little studied in the Rhône, which brings a novelty factor. Besides, works from other hydrosystems (Nylund et al., 1992, Zegers et al., 2003, Muir and Rose, 2007) suggest that they have consistent and more contemporary temporal trends, meaning that they could potentially be used as a time-marker for recent sediment records.

The following organic contaminants were quantified in the LABERCA laboratory (ONIRIS Nantes, France):

- The seven indicator PCB congeners: PCB 28, 52, 101, 118, 138, 153, 180, of which the sum is further referred to as ∑7PCBi on cores PDR-1902, PDR-1802, PDR-1806 and PDR-C10a;
- Nine PBDE congeners: PBDE 28, 47, 49, 99, 100, 153, 154, 183, and 209, of which the sum is further referred to as ∑9PBDE on cores PDR-1902, PDR-1802 and PDR-1806;

The samples were collected at a step of 4 cm, packaged in amber glass vials and then sent to the LABERCA laboratory for further analysis. After freeze-drying, extraction and purification procedures, all persistent organic pollutants (POPs) analyses were simultaneously carried out by gas chromatography coupled with high-resolution mass spectrometry (GC/HRMS) using a 7890A gas chromatograph (Agilent) coupled with a JMS 800D double-sector high-resolution mass spectrometer

(JEOL, Tokyo, Japan). The quantification was ensured by isotopic dilution using 7 ^{13}C-labeled internal PCB standards and 9 ^{13}C-labeled internal PBDE standards added to the samples before the extraction step. A thorough description of the analysis protocol can be found in Vénisseau et al. (2015) and Liber et al. (2019). The limits of detection (LOD) for PCBs range from 0.049 (PCB 118) to 0.109 (PCB 28) µg·kg^{-1} DW and for PBDEs from 0.002 (PBDE 28) to 0.05 (PBDE 183) µg·kg^{-1} DW. The recoveries range from 60 to 120%.

2.3.4. Sediment dating

Cesium-137 (^{137}Cs) was assessed on cores PDR-1802, PDR-1806, PDR-1902 and PDR-C10a. This anthropogenic radionuclide is typically used to identify two events that appear as peaks in the radionuclide activity: nuclear weapon testing in 1962-1963 (Ritchie and McHenry, 1990) and the Chernobyl accident in 1986. Additionally, excess lead-210 (^{210}Pb$_{xs}$) activity was assessed on core PDR-1902 only. ^{210}Pb is a natural radionuclide that is part of the uranium-238 radioactive decay series and is continually supplied to sediments from atmospheric deposition. Excess ^{210}Pb radioactive decay can be used to model sediment accumulation rate in a sediment core –and by extension, date it- assuming that the sediments have not been subjected to large scale disturbances (Baskaran et al., 2014). We assumed that there was neither mixing nor diffusion of ^{210}Pb$_{xs}$ in the core and therefore used the Constant Flux Constant Sedimentation model in this study (Krishnaswamy et al., 1971; Bruel and Sabatier, 2020).

Samples were collected at steps of 4 to 8 cm, dried for 48h at 40°C and preserved in polystyrene boxes. Sub-samples from each core were analyzed by counting for at least 24h, using low-background gamma spectrometry. Gamma emissions were detected with a germanium detector and used to quantify specific activities of ^{226}Ra, ^{228}Ra, ^{40}K, ^{210}Pb, and ^{137}Cs. Those analyses were carried out in the LMRE laboratory (Laboratoire de Métrologie de la Radioactivité dans l'Environnement, IRSN, Orsay) for cores PDR-C10a, PDR-1802 and PDR-1806, and in the LSCE laboratory (Laboratoire des Sciences du Climat et de l'Environnement, Gif-sur-Yvette, France) for core PDR-1902. The mean detection limit is 0.1 Bq.

Age-depth modelling was carried out on cores PDR-1802, PDR-1806, PDR-1902 and PDR-C10a using the R package "clam" (Classical Age-Depth Modelling of Cores from Deposits) v.2.3.4 (Blaauw, 2010). Two models were developed:

- Model M1 uses only the most robust time-markers i.e. the surface (date of sampling), ^{137}Cs or ^{210}Pb trends and abrupt grain-size events associated with dated hydrological or human-driven events.
- Model M2 uses the time-markers from model M1 as well as additional time-markers linked to PCB and PBDE trends (e.g. date of early use of a contaminant, date of restriction of use, date of ban, etc.).

The point in developing those two models was to assess whether contaminant trends can be used as reliable time-markers in this context and whether they might allow to increase the dating accuracy. The model type (e.g. linear regression, linear interpolation, etc.) was chosen for each core as to obtain the best possible goodness of fit. The model type and parameter inputs for each model are available in Supplementary Information (Table S2).

3. Results

3.1. Physical characteristics of the depositional environments

The bathymetric measurements of a transect of the Saint-Pierre-de-Boeuf dam reservoir over time are featured in Supplementary Information (Fig. S1). They show the progressive filling of the recess zone on the right bank side (between roughly 100 and 300 m). In 1980 (two years after the dam implementation in 1978), the old channel could still be distinguished around 150-200 m. The major part of the filling (up to 6.5 m of sediments deposited) happened between 1980 and 1999. Since 1999, up to one additional metre accumulated in the recess zone. Core PDR-1902 was sampled in this zone, around 150 m on the measured transect. Its compaction rate could not be measured and therefore had to be assumed; based on previous underwater cores, a 30% rate was used for the representation

in Fig. S1. The high uncertainty associated with the compaction rate of core PDR-1902 means that the bathymetric measurements cannot be used as absolute time-markers. However, they still suggest that the bottom of the core is older than 1999.

The Ilon (active) secondary channel is approximately 20 m large, 300 m long and with a water depth depending on the season but generally around 1 m. The longitudinal survey GPR12 (Fig. 2.a) shows that more than 5 m of sediments accumulated in the channel overtime. A continuous subparallel reflector can be observed along the whole profile around 2-2.5 m. It might correspond to the original gravel bed of the channel (before 1860, cf. section 2.1). The filling above this reflector is rather homogeneous with mostly subparallel and sinuous reflectors, indicating a continuous deposition with little to no reworking. A close-up on the part of the transect where the sediment cores are located allows to distinguish a continuous sinuous reflector that matches with a grain-size limit observed in sediment cores PDR-1802 and PDR-1805 (see section 3.2 for more details), proving the consistency between GPR observations and the results from the core sampling. The survey shows that although one core is 94 cm-long while the other is 57 cm-long, they deposited roughly in the same time span, meaning sediment accumulation rates may vary a lot inside this compartment. This variability is inherent to fluvial sediment deposition and has to be considered for a correct interpretation of sediment records, which demonstrates the interest of combining sediment cores with geophysical surveys.

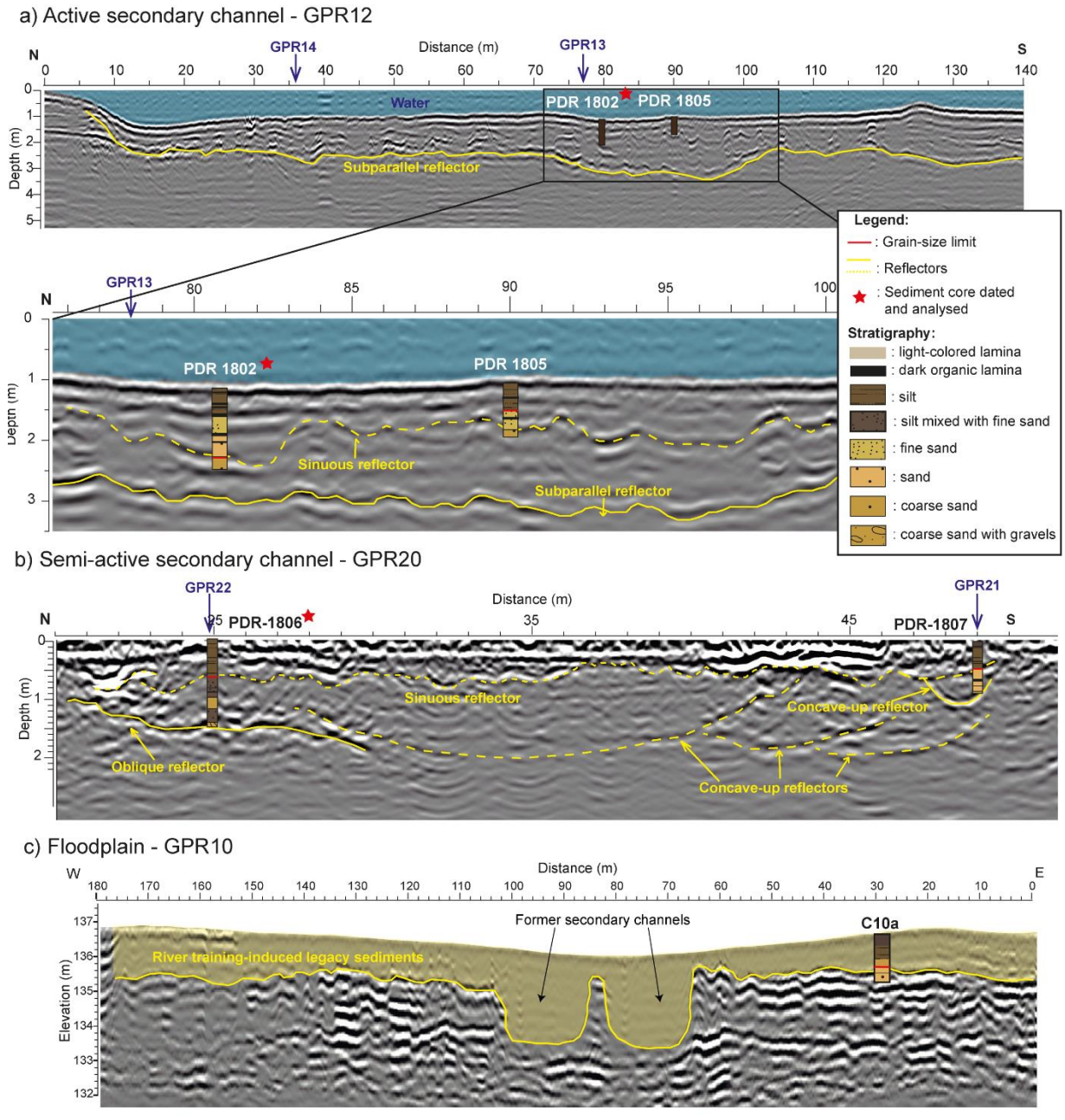

299

300 *Figure 2: Interpreted Ground Penetrating Radar surveys with sediment cores positioned; a) GPR12 from the active secondary*
301 *channel; b) GPR20 from the semi-active secondary channel; c) GPR10 from the floodplain. NB: Other transversal GPR surveys*
302 *for the active secondary channel (GPR21, GPR22) and the semi-active secondary channel (GPR13, GPR14) are available in*
303 *Supplementary Information (Fig. S2).* [IN COLOR]

304 The Limony secondary channel is approximately 20 m-large and 1 km-long, although the geophysical
305 surveys and sediment cores are only located in the last 200 m downstream of the channel (Fig. 1.d).
306 The longitudinal transect GPR20 (Fig. 2.b) shows multiple oblique and concave-up reflectors between
307 depths of 0.5 and 2 m. They may be the result of strong and multiple erosion dynamics, indicating that

the channel used to have an important bed mobility. The bottoms of both sediment cores (PDR-1806 and PDR-1807) match with reflectors, which shows again the consistency between the two methods. Around 50 cm, a rather continuous and sinuous reflector can be identified all along the survey. The sediment filling above this reflector is more homogeneous, hinting at calmer depositional processes.

GPR12 from the floodplain compartment is roughly perpendicular to the Rhône main channel axis. A very clear continuous reflector can be observed all along the survey (Fig. 2.c), outlining two former secondary channels that have been entirely filled in and are not discernible nowadays from the surface. Other subparallel reflectors are apparent below the continuous reflector while the GPR image is smooth above: this filling is characteristic of legacy sediments induced by the implementation of river training infrastructures in the 1880s in the area, as demonstrated in Vauclin et al. (2020). The continuous reflector also coincides with a grain-size limit observed in the corresponding sediment core (PDR-C10a).

3.2. Grain-size characteristics of the sediment cores

The cores from the dam reservoir (PDR-1901 and PDR-1902) are almost exclusively comprised of silt, with only a few centimetres of very fine sand at their bottom. At their opening, they exhibited organic macro-remains and dark organic laminas, as well as a few light-coloured laminas. The cores retrieved in secondary channels (PDR-1802, PDR-1805, PDR-1806, PDR-1807) have a similar stratigraphic description: an upward fining pattern of coarse sand, fine sand and silt from the bottom to the top of the cores (Fig. 3). They also had many noticeable organic macro-remains (leaves, seeds, shells, etc.) and several darker laminas. The core from the floodplain (PDR-C10a) is characterized by silty deposits in its top 75 cm and sands at the bottom.

The grain-size heatmaps (Fig. 3) from the cores from the dam reservoir highlight a very homogeneous grain-size distribution, only comprised of fine (D50~20 µm) and poorly sorted sediments. In contrast, two main sections can be distinguished in the cores from the active channel: the top sediments are fine (D50~20-50 µm) and poorly classified (i.e. the distribution is widely spread around the D50), while

the sediments at the bottom of the cores are coarser (D50~200 µm) and well-sorted (i.e. the distribution is closely centred around the D50). This change in grain-size characteristics can be observed at 80 cm and 42 cm on PDR-1802 and PDR-1805 respectively (Fig. 3). A similar grain-size limit can be identified on the heatmaps of the cores from the semi-active secondary channel, at 48 and 40 cm in cores PDR-1806 and PDR-1807 respectively. The transition between the two grain-size patterns is sharp and is represented as a dotted red line on Fig. 3. A similar distinction between the top (fine, poorly sorted sediments) and the bottom (coarser, well-sorted sediments) can be observed in core PDR-C10a from the floodplain environment. The corresponding grain-size limit has already been analysed in Vauclin et al. (2019) and has been identified as the result of the implementation of river training infrastructures in the 1880s.

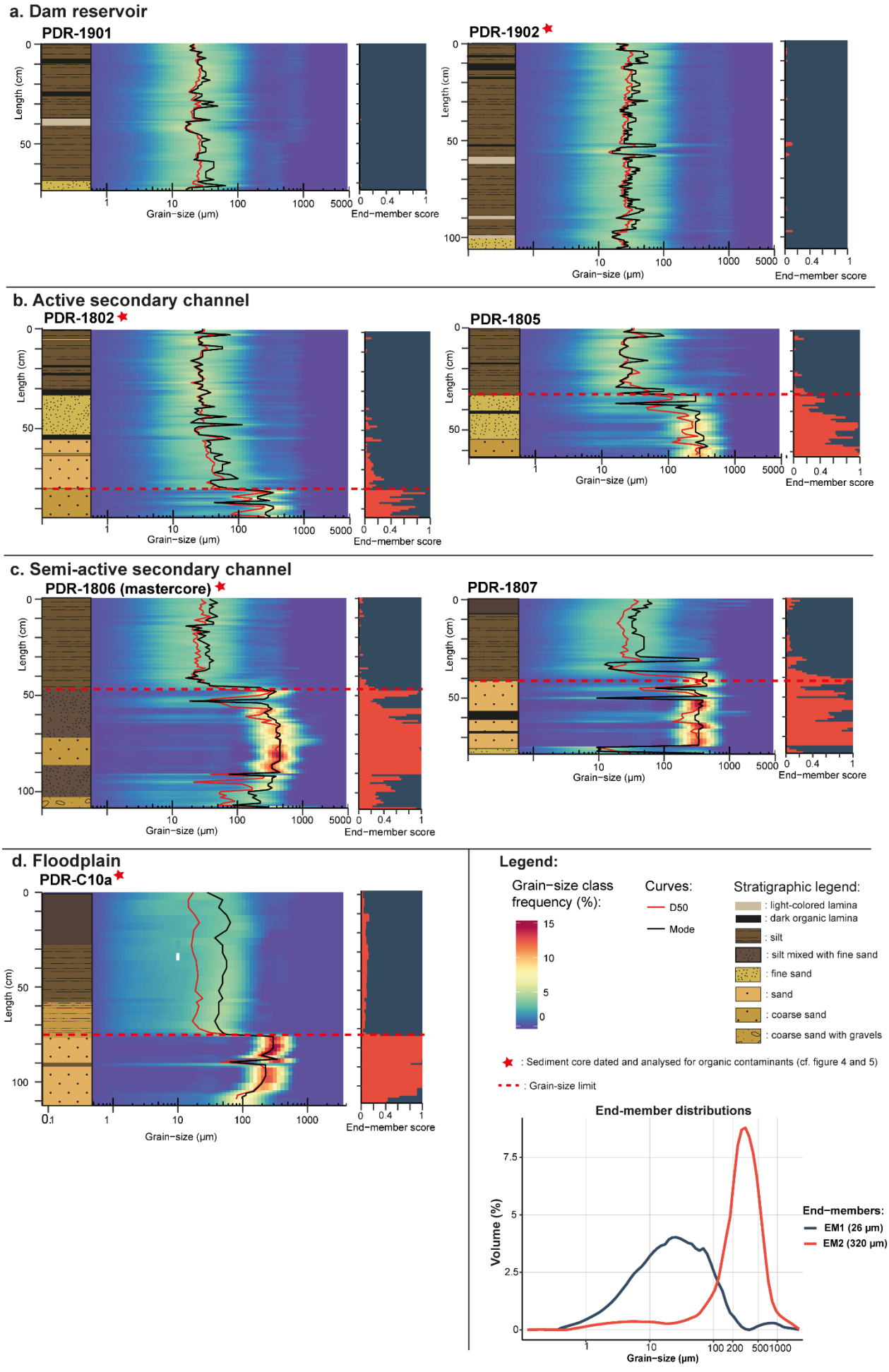
a. Dam reservoir
PDR-1901
PDR-1902
b. Active secondary channel
PDR-1802
PDR-1805
c. Semi-active secondary channel
PDR-1806 (mastercore)
PDR-1807
d. Floodplain
PDR-C10a
Length (cm)
Grain-size (µm)
End-member score
Legend:
Grain-size class frequency (%):
Curves:
D50
Mode
Stratigraphic legend:
: light-colored lamina
: dark organic lamina
: silt
: silt mixed with fine sand
: fine sand
: sand
: coarse sand
: coarse sand with gravels
: Sediment core dated and analysed for organic contaminants (cf. figure 4 and 5)
: Grain-size limit
End-member distributions
Volume (%)
End-members:
EM1 (26 µm)
EM2 (320 µm)

Figure 3: Grain-size characteristics for the seven studied sediment cores in a) the dam reservoir, b) the active secondary channel (Ilon), c) the semi-active secondary channel (Limony), and d) the floodplain. For each core, from left to right: stratigraphic description, heatmap representation of the total grain-size repartition and End-Member scores. [IN COLOR]

The End-Member Modelling Analysis (EMMA) algorithm (Dietze et al., 2012) showed that the corpus of grain-size distributions (GSDs) was best represented with two end-members (EM). The main modes are at 26 and 320 µm and represent each around 50% of the grain-size distributions (Fig. 3). This end-member model has a class-wise explained variance of 52% and a sample-wise explained variance of 93%.

The end-member scores –i.e. their percentage of representation of the GSDs- vary depending on the sediment core and the depth of the sample (Fig. 3). In the reservoir cores (PDR-1901 and PDR-1902) and in the top part of the 5 other cores, EM1 is largely predominant, which is consistent with the fine homogeneous sediments observed in the stratigraphic descriptions and heatmaps. Below the grain-size limit, EM2 is mostly represented which corresponds to the observed sandy sediments. The grain-size limit identified in the heatmaps can be clearly seen on the end-member score graphs as well. It appears as an abrupt change in the EMs repartition and supports the observation that there is a sudden change in the grain-size properties that can be consistently observed all sediment cores except those from the dam reservoir, and might therefore be linked to river engineering. While this limit was initially derived from visual observations and grain-size data, the fact that it also appears in the EM score graphs gives it a statistical weight. Overall, the end-member modelling attests of the existence of two distinct deposition processes in the studied cores: EM1 is likely representative of a decantation process in a context of still waters, while EM2 might represent former dynamics of deposition from when the fluvial corridor was not constrained by the various engineering works.

3.3. Vertical trends in the geochemical characteristics of the sediments

3.3.1. Vertical trends in Total Organic Carbon

The Total Organic Carbon (TOC) contents in the cores (Fig. 4) are comprised between 0 and 5%. The vertical trend in TOC in PDR-1902 (dam reservoir, Fig. 4.a) is monotonous at around 2%. In PDR-1802, the TOC is low (<1%) before the grain-size rupture (active secondary channel, Fig. 4.b), then increases up to 3% at 55 cm, before falling back at ~2% until the surface. In PDR-1806 (semi-active channel, Fig. 4.c), the TOC content is null in the bottom of the core until ~50 cm from the top. It then increases up to 4-5% close to the surface. In PDR-C10a (floodplain, Fig. 4.d), the TOC is almost null below 75 cm, increases slowly towards the surface, and then more sharply in the last ten centimeters. It is worth noting that the increase in TOC systematically coincides with the grain-size ruptures identified previously (red dotted line in Fig. 4) in all cores.

3.3.2. Vertical trends in persistent organic pollutants

In core PDR-1902 (dam reservoir, Fig. 4.a), the Σ7PCBi concentration follows a decreasing trend from the bottom (~40 µg kg^{-1}) to the top (~10-20 µg kg^{-1}). Two sharp peaks can however be observed at 78 cm (120 µg kg^{-1}) and 12 cm (40 µg kg^{-1}). The Σ9PBDE concentration starts around 200 µg kg^{-1} at the very bottom of the core, peaks at ~400 µg kg^{-1} at 96 cm and then decreases steadily from 200 µg kg^{-1} at 90 cm to ~20 µg kg^{-1} close to the surface. The TOC normalization does not significantly modify the observed trends in this core.

In core PDR-1802 (active secondary channel, Fig. 4.b), the Σ7PCBi concentration is around 80 µg.kg^{-1} at the very bottom of the core and fluctuates between ~40 and 90 µg kg^{-1} until 50 cm. It then decreases steadily to reach a stable value of 20 µg kg^{-1} close to the surface. When normalizing the Σ7PCBi concentration to the TOC (in order to remove a potential confounding effect due to the affinity of persistent organic pollutants for organic matter), the trend is significantly modified: we observe an exponential decrease in Σ7PCBi/TOC from the bottom of the core to the surface. The Σ9PBDE concentration is null at the very bottom but increases rapidly and peaks at ~250 µg kg^{-1} around 50 cm.

391 It decreases then steadily to reach ~25 μg kg^{-1} at the surface. The TOC normalization does not change

392 significantly the overall vertical trend observed for PBDEs.

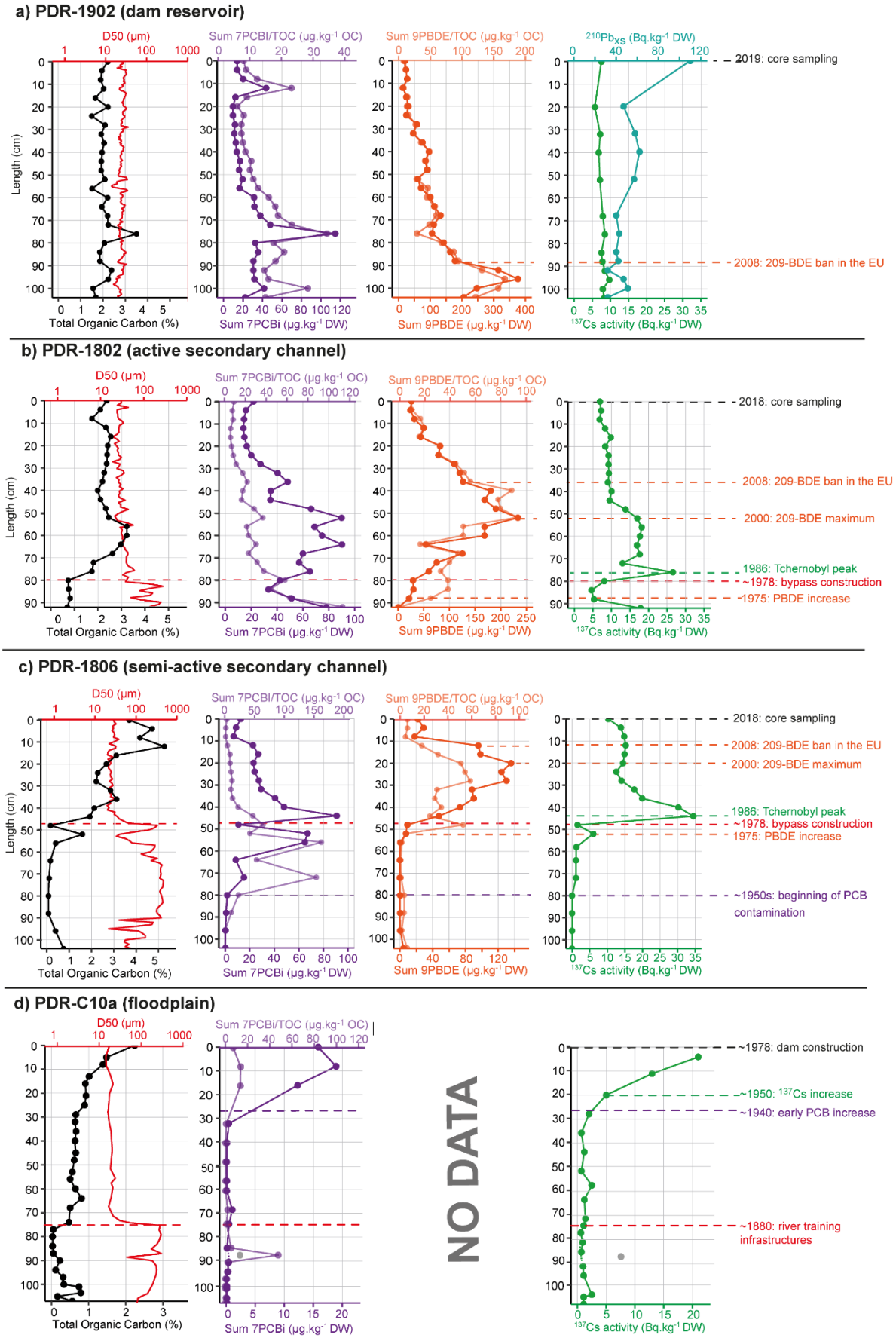
a) PDR-1902 (dam reservoir)
D50 (µm)
Sum 7PCBI/TOC (µg.kg-1 OC)
Sum 9PBDE/TOC (µg.kg-1 OC)
210Pbxs (Bq.kg-1 DW)
Length (cm)
Total Organic Carbon (%)
Sum 7PCBi (µg.kg-1 DW)
Sum 9PBDE (µg.kg-1 DW)
137Cs activity (Bq.kg-1 DW)
2019: core sampling
2008: 209-BDE ban in the EU
b) PDR-1802 (active secondary channel)
2018: core sampling
2008: 209-BDE ban in the EU
2000: 209-BDE maximum
1986: Tchernobyl peak
~1978: bypass construction
~1975: PBDE increase
c) PDR-1806 (semi-active secondary channel)
2018: core sampling
2008: 209-BDE ban in the EU
2000: 209-BDE maximum
1986: Tchernobyl peak
~1978: bypass construction
1975: PBDE increase
~1950s: beginning of PCB contamination
d) PDR-C10a (floodplain)
NO DATA
~1978: dam construction
~1950: 137Cs increase
~1940: early PCB increase
~1880: river training infrastructures

393

Figure 4: Vertical trends in geochemical characteristics in cores a) PDR-1902; b) PDR-1806; c) PDR-1802; d) PDR-C10a. For each core, the following characteristics are presented from left to right: Total Organic Carbon (TOC) content, D50, sum of the 7 indicator PCBi, sum of 9 PBDE, ^{137}Cs activity. For organic contaminants, the darkest curve represents the raw concentrations while the lightest curve represents the concentrations normalized to the TOC. NB: the sum of 9PBDE was not measured in core PDR-C10a. [IN COLOR]

The Σ7PCBi concentration is null in the bottom part of core PDR-1806 (semi-active channel, Fig. 4.c) but increases quickly starting at 80 cm from the surface. It peaks at a value of ~100 µg kg^{-1} at 44 cm, then decreases steadily to reach a background value of ~5-10 µg kg^{-1} close to the surface. When normalizing the Σ7PCBi concentration to the TOC, the vertical trend is significantly modified: the increase is sharper starting at 80 cm, and the peak happens lower in the core, between roughly 55 and 70 cm. From 55 cm to the surface, an exponential decrease is then observed. In this core, the Σ9PBDE concentration is null between the bottom of the core and ~50 cm from the surface. We can then observe a sharp increase in concentration until ~140 µg kg^{-1} around 20-30 cm. Starting at 20 cm, the concentration decreases rapidly until 20-30 µg kg^{-1} close to the surface. The TOC normalization does not significantly impact the PBDEs vertical trend.

In core PDR-C10a (floodplain, Fig. 4.d), the Σ7PCBi concentration is null in the bottom part of the core. The first measured concentration is ~12 µg kg^{-1} around 18 cm, and the contamination levels then stay similar until the surface. The TOC normalization shows that the contamination is minimal compared to the other cores but does not modify the tendency.

It is worth specifying that the congener repartition for PCBs and PBDEs is similar in all three cores and does not vary significantly with depth. The highly chlorinated PCB congeners (PCB-138/PCB153/PCB180) are predominant, generally representing between 60 and 80% of the Σ7PCBi. Meanwhile, congener 209 (BDE-209, the main component of the deca-BDE commercial mixture) represents between 93 and 99% of the Σ9PBDE measured in the samples and was therefore mainly considered in further interpretations.

3.3.3. Radionuclides activity trends

The ^{137}Cs activity profile for core PDR-1902 (dam reservoir, Fig. 4.a) is monotonous and comprised of background values between 5 and 10 Bq kg^{-1}. No activity peak is observed. The $^{210}Pb_{xs}$ activity profile globally decreases from ~120 Bq kg^{-1} at the top to 40-60 Bq kg^{-1} at the bottom of the core. While a few measure points slightly deviate from that decreasing trend (e.g. at 20 cm), all were nevertheless taken into account for the modelling.

In core PDR-1802 (active secondary channel, Fig. 4.b), the ^{137}Cs activity is around 20 Bq kg^{-1} at the very bottom of the core and decreases onto the last 8 cm. This declining trend hints at the existence of an earlier peak that was not recorded in the core. The activity then increases to peak at 25 Bq kg^{-1} around 76 cm. Afterwards, it decreases quickly between 44 and 78 cm, and more progressively between 44 cm and the surface, where the activity stalls around 5 Bq kg^{-1}.

The ^{137}Cs activity in core PDR-1806 (semi-active secondary channel, Fig. 4.c) is null from the bottom of the core to 80 cm from the surface, then very low (<5 Bq kg^{-1}) until 58 cm. We can then observe two activity peaks of different intensities: a 6 Bq kg^{-1} peak at 52 cm, followed by a temporary decrease and more straightforward peak of 35 Bq kg^{-1} at 44 cm. Above this second peak, the ^{137}Cs activity decreases overall to reach 10 Bq.kg^{-1} at the surface, although a slight increasing trend can be observed again between 12 and 25 cm.

In core PDR-C10a (floodplain, Fig. 4.d), ^{137}Cs activity is null in the bottom of the core and increases from 20 cm onwards. It starts at around 5 Bq kg^{-1} and reaches 20 Bq kg^{-1} close to the surface.

3.4. Age-depth modelling

3.4.1. Date markers

The grain-size change identified in cores from the secondary channels (PDR-1802 and PDR-1806; cf. section 3.3) and the floodplain (PDR-C10a) can be used as a date marker. Indeed, a similar change has already been observed in sediment cores from the Rhône floodplain, in this study area and two other sites along the river corridor (Vauclin et al., 2019; Vauclin et al., 2020). In those cases, it was proven

444 that the abrupt grain-size modification was due to the first period of river engineering (~1880) that
445 created a partial disconnection between the channel and the floodplain, and sediments above the limit
446 were therefore defined as infrastructure-induced legacy sediments. This mechanism is illustrated here
447 in the floodplain core (PDR-C10a). In the cores from the secondary channels, however, the grain-size
448 change is located just below ^{137}Cs activity peaks and therefore has to be more contemporary than the
449 1880s. We therefore concluded that it was caused by the second period of river engineering (bypass
450 implementation) in 1978. As a consequence, we considered that the ^{137}Cs activity peaks in cores PDR-
451 1802 and PDR-1806 were the result of the 1986 Tchernobyl accident since both are located above the
452 1978 grain-size limit.

453 Tipping points in organic contaminants trends were used as secondary date markers in models M2 (in
454 addition to absolute date-markers, cf. section 2.3.4), based on production/consumption temporal data
455 or already published dated contamination trends from other sedimentary archives. Standard errors
456 were associated with POPs time-markers to take into account the lag time between the legislation, its
457 implementation at the national scale and the time needed to record a decrease in the sediment record
458 (Table S2). All date markers used in this study and their justification and/or reference are available in
459 Table 1.

Date marker	**Date**	**Sediment cores**	**Reference/explanation**
Absolute date markers			
^{137}Cs activity peak	1986	PDR-1806, PDR-1802	See section 3.5.1
Grain-size change	1978	PDR-1806, PDR-1802	See section 3.5.1
Secondary date markers			
PCB concentration increase	1950	PDR-1806	Breivik et al., 2002b; Desmet et al., 2012; Lorgeoux et al., 2016; Dendievel et al., 2020

PBDE concentration increase	1975	PDR-1806, PDR-1802	Nylund et al., 1992; Muir and Rose, 2007; Kohler et al., 2008; Lorgeoux et al., 2016; Abbasi et al., 2019
209-BDE maximum	2000	PDR-1806, PDR-1802	Kohler et al., 2008; Abbasi et al., 2019
209-BDE ban in the EU	2008	PDR-1806, PDR-1802, PDR-1902	European Parliament, 2002/95/CE, European Court of Justice ruling, April 1st 2008

Table 1: Date markers used to build the age-depth models

3.4.2. Age models

Model M1 for core PDR-1902 was developed from ^{210}Pbxs modelling exclusively. The coefficient of determination of the model was R^2=0.61, and the resulting sedimentation rate in the reservoir computed from the regression slope is 4.12 cm yr^{-1}. According to this model, the bottom of core PDR-1902 would date back to 1993 (Fig. 5.a). Model M2 additionally considers the PBDE decreasing trend in the core and results from a linear regression. It estimates a constant sedimentation rate of 5.0 cm yr^{-1} in the reservoir, the bottom of the core therefore dating back to 1999. While both models give relatively similar results, the bathymetric measurements (Fig. S2) suggest that the bottom of the core is older than 1999, which renders model M1 more plausible.

Models M1 and M2 for core PDR-1802 were obtained with a linear interpolation model (Fig. 5.b). According to model M1, the bottom of the core dates back from 1960. The resulting sedimentation rate is around 2.3 cm yr^{-1} between 1986 and 2018. Model M2 gives very similar results to model M1: the date of the bottom of the core is estimated at 1969 and the sedimentation rate is around ~1.2 cm.$year^{-1}$ until 1986, 1.7-1.8 cm yr^{-1} between 1986 and 2006 and 3.2 cm yr^{-1} between 2006 and the surface. The consistency between the two models suggest that the dating of core PDR-1802 is overall valid, although the dating of very bottom of the core beyond the older time-marker should be

considered with caution as the results had to be extrapolated. This also indicates that the additional time-markers linked to the PBDE contamination trend in model M2 are reliable in this case.

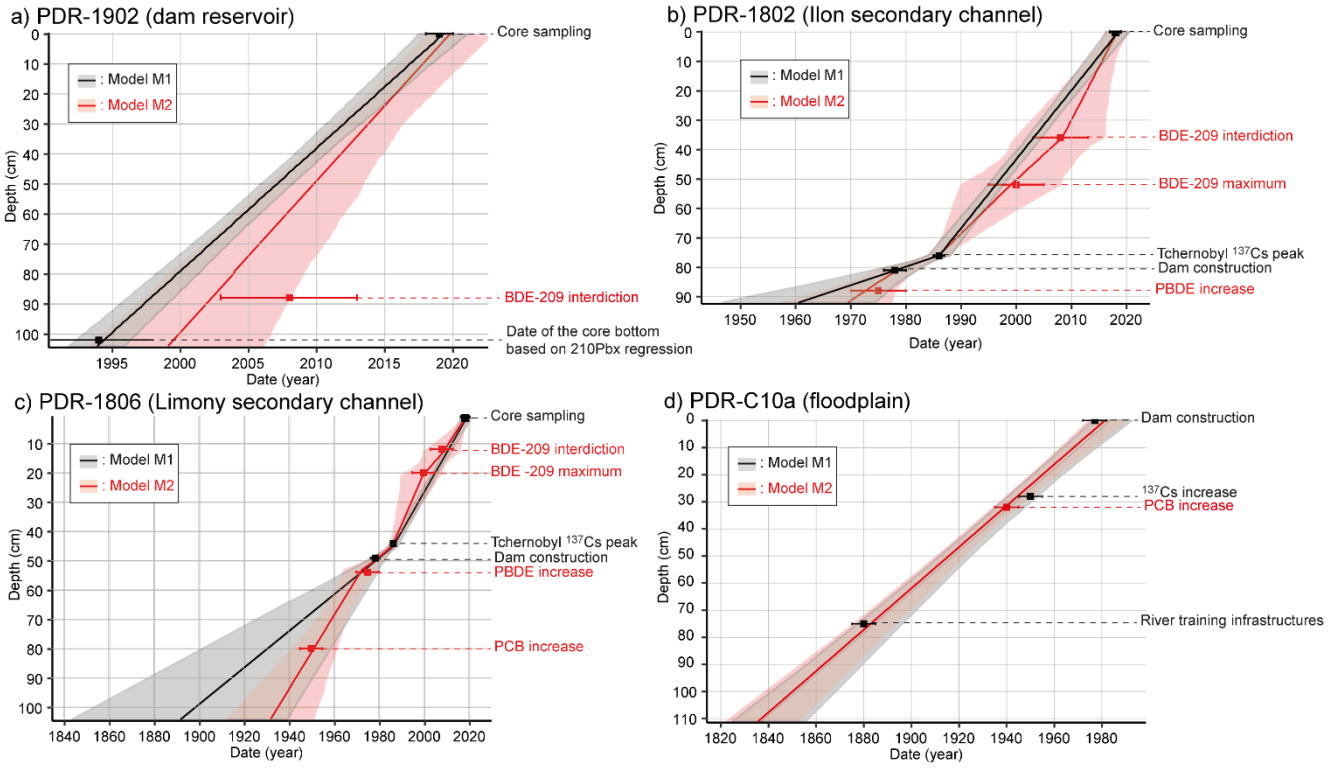

Figure 5: Age-depth models for cores PDR-1902, PDR-1802, PDR-1806 and PDR-C10a. [IN COLOR]

Models M1 and M2 fore core PDR-1806 were obtained with a linear interpolation model (Fig. 5.c). According to model M1, the bottom of the core dates back from 1890, however this date results from a large extrapolation -the latest time-marker being positioned at 48 cm- and is therefore unreliable. The sedimentation rate is estimated at 0.6 cm yr^{-1} between the bottom of the core and 48 cm (time-marker: ^{137}Cs peak 1986), then increases at 1.3 cm yr^{-1} until the surface. Model M2 gives a very similar estimation for the top 48 cm of the core, with a sedimentation rate comprised between 1 and 2 cm yr^{-1} between 1986 and 2018. Between 50 and 104 cm, however, the slope of the modelled line is steeper, with an estimated 1.4 cm yr^{-1} sedimentation rate. According to this model, the bottom of the core dates back from 1933, although it should still be considered with caution as it results from extrapolation. As the two models give consistent results for the top 48 cm of the core, we can assume that the dating of this section is reliable. The two additional time-markers related to the PBDE

492 contamination trend in model M2 therefore appear as accurate. Regarding the bottom half of the core,
493 model M2 is likely the most accurate of the two, as the beginning of PCB contamination in sediments
494 is widely accepted as dating back from the early 1950s (Wania, 1999; Breivik et al., 2002a; Breivik et
495 al., 2002b) and such a trend has already been observed in sediment core from the Rhône River (Desmet
496 et al., 2012; Mourier et al., 2014).

497 The best results for the age-depth modelling of core PDR-C10a (Fig. 5.d) were obtained with a linear
498 regression model. Only one POPs time-marker is additionally used in model M2 compared to M1,
499 therefore the two models are practically identical. A consistent sedimentation rate of 0.76 cm yr^{-1} is
500 estimated in both cases, with the bottom of the core dating back from 1840. However, the last reliable
501 time-marker is the grain-size change resulting from the river training infrastructures implementation
502 in the area around 1880, at 75 cm. Below this point, the model results are highly uncertain as they
503 stem from extrapolation.

504 # 4. Discussion

505 ## 4.1. Multi-proxy dating in a complex fluvial setting

506 Dating often constitutes the basis for the interpretation of other information recorded in a sediment
507 sequence, such as identifying contamination trends or relating grain-size patterns to hydrological
508 events. However, achieving a robust dating of sediments from a complex fluvial setting is challenging
509 and requires extensive interpretation in its own. Two types of dating methods can be distinguished
510 based on the information they provide (Notebaert et al., 2011): discrete methods such as radiocarbon,
511 Optically Stimulated Luminescence or ^{137}Cs will provide an absolute date for a few discrete points in
512 the core, while continuous methods based on the presence and evolution of tracers -for instance
513 contaminant trends- will allow to identify time periods based on their vertical repartition in the
514 deposits. In fluvial contexts, several processes might render these dating methods ambiguous:
515 sedimentation hiatuses due to incision, erosion, or the intermittent nature of a depositional
516 environment (e.g. floodplain), fluctuations of sediment accumulation rate, post-depositional processes

517 (e.g. bioturbation, contaminants/radionuclides migration or leeching), etc. (Lewin and Macklin, 2003;
518 Bábek et al., 2008; Matys Grygar et al., 2016). The different dating methods will be more or less
519 affected by those processes: the use of ^{137}Cs activity measurements might prove little informative if a
520 sedimentation hiatus coincides with an activity peak or if the sediments were deposited after 1986,
521 while a varying sedimentation rate is especially misleading when trying to infer a time period from a
522 known contamination trend.

523 A combination of complementary methods is therefore optimal for a robust dating of a sediment
524 sequence in a complex fluvial system, as illustrated in this study where no less than five types of time-
525 markers (^{137}Cs and ^{210}Pb activity, contamination trends, grain-size changes, bathymetric
526 measurements) were necessary to build reliable age-depth models for each of the four depositional
527 environments. Indeed, few discrete time-markers were available in our samples: the deposits are too
528 recent for radiocarbon dating to give relevant results, and clear ^{137}Cs peaks could only be identified in
529 two out of the four depositional environments. We therefore had to use continuous and less robust
530 indicators such as contamination trends. PCBs temporal trends in sediments are reasonably well-
531 known, having been studied in many European Rivers (Bábek et al., 2008; Malina et Mazlova, 2017;
532 Lorgeoux et al., 2016, Dendievel et al., 2020) including the Rhône River (Desmet et al., 2012, Mourier
533 et al., 2014). They started being produced in the 1930s but the contamination often appears in
534 sediments from the 1950s only (Lorgeoux et al., 2016, Dendievel et al., 2020). Their emissions peaked
535 in 1975 in France (Breivik et al., 2002b), which coincides with the prohibition of their use in open
536 systems, and then decreased. They were then banned from use and sale in closed system as well in
537 1987. In our case, unfortunately, only core PDR-1806 recorded the complete PCB temporal trend, and
538 the large discrepancy between the concentration and the TOC-normalized trends (Fig. 4.b) rendered
539 unreliable any date indication other than the initial increase in concentrations (~1950s). PBDEs have
540 been less investigated and there is no consensus yet about their temporal repartition in sediment
541 deposits. However, their concentrations follow a well-defined pattern that seems consistent in the
542 cores from the aquatic environments (Fig. 4.a, 4.b and 4.c), meaning they could be used as geochemical

543 tracer. As for PCBs, their use is restricted in time: they started being produced in 1970 (Lauzent, 2017),
544 and were progressively banned from use and production by the European Union from 2004 to 2008
545 (European Parliament, 2002/95/CE). Additionally, results from dated sediment cores (Nylund et al.,
546 1992, Zegers et al., 2003, Muir and Rose, 2007) suggest a contamination peak in the early to late 1990s
547 depending on the congener, BDE-209 tending to peak in the early 2000s as the use of the deca-mix
548 was regulated later than the others.

549 Relying on contamination trends -especially ones that were less studied- is risky to date sediment
550 archives in such a complex setting, therefore our approach was to construct two separate age-depth
551 models for the aquatic cores: model M1 from the absolute time-markers only (^{137}Cs, grain-size changes,
552 sampling date), inevitably imprecise but reliable; and model M2 using contamination trends as
553 additional time-markers. Both models ended up being similar in the four cores, which proves the
554 robustness of our approach. In the case of PDR-1806, the use of PCBs contamination trend even
555 allowed to significantly improve the age-depth model in the lowest part of the core. This methodology
556 also confirms the potential for PBDE contamination trends to be increasingly used as time-markers in
557 sediment deposits, although larger-scale studies would be useful to ascertain it. Finally, the lack of
558 time-markers in the most recent core (PDR-1902, Fig. 4.a) highlights the interest of investigating
559 emergent contaminants trends in order to retain the ability to date future sediment cores where
560 conventional date-markers such as ^{137}Cs peaks and historical organic contaminants may not be
561 present.

562 4.2. Characterization of the depositional environments

563 One of the aims of this study is to demonstrate that a thorough characterization of the fluvial
564 depositional environment from which a sediment core will be sampled is essential and time efficient.
565 While the four depositional environments have been previously described from a geographical and
566 geophysical point of view, this section intends to formally characterize these environments based on

567 previous geomorphology studies and illustrate incidentally the interest of such characterization for
568 sediment archive interpretation.

569 The dam reservoir environment in this study cannot readily be compared to most reservoirs in terms
570 of depositional processes, as the run-of-river dam is punctually erased during floods and few sediments
571 are therefore deposited in the axis of the dam (Fig. S2). The coring zone where sediments accumulated
572 corresponds to a recess zone where there is little flow velocity under normal discharge conditions and
573 is likely closer to a harbour basin in terms of context. The environment was never dredged and there
574 is no sedimentological nor bathymetric evidence to show that sediment remobilization might have
575 happened during floods: the core sediments are fine (silt to clay) and homogeneous, and the
576 bathymetric lines are in chronological order. Few date markers were available in the core sampled in
577 the reservoir, which renders essential the knowledge that sedimentation is likely continuous and
578 sustained in time in this environment: it supports the use of ^{210}Pbxs decay and a linear regression age-
579 depth modelling to establish the chronology of the core.

580 The Ilon (active) secondary channel was affected by the river training phase in the 1880s: the upstream
581 end of the larger secondary channel to which the Ilon channel is connected to was barred by a dyke
582 (Vauclin et al., 2019, Tena et al., 2020). Later on, the dam implementation quickly resulted in the
583 disconnection and siltation of the upstream part of the channel, which is a common consequence of
584 bypassing in the Rhône River as demonstrated in Dépret et al. (2019). Both phases can be identified
585 on the GPR profile due to a distinct and continuous subparallel reflector (dotted line on Fig. 2.a) that
586 matches temporally with the dam-induced legacy sediment limit in the cores (Fig. 3.b). While the grain-
587 size analysis shows that sediments below the limit are coarser (fine sand) than those above (silt), both
588 units appear similar on the GPR survey: poorly defined subparallel reflectors that are indicative of a
589 calm deposition process. A deeper subparallel reflector is speculated to correspond to the pre-
590 infrastructure gravel-bed (Fig. 2.a). Overall, this depositional environment is therefore characteristic
591 of a passive channel fill (Aslan, 2013). The river training infrastructure initiated the filling, and the

severe flow reduction associated with bypassing emphasized the disconnection, resulting in the deposition of finer sediment without altering the sedimentary architecture. Understanding the chronology of the filling process of this environment was invaluable to reinforce the dating of the corresponding sediment core.

The Limony (semi-active) secondary channel was artificially disconnected from the main channel by the building of dykes at its upstream and downstream ends in the 1880s (Vauclin et al., 2019; Tena et al., 2020). Both the sediment cores and the GPR results prove that two distinct phases of infilling followed. The first phase is characterized by numerous oblique and concave reflectors on the GPR profile (Fig. 2.b) and fine to medium sands in the corresponding section of the sediment cores (Fig. 3.c). Both aspects are indicative of an active fill (Aslan, 2013), with deposition of bedload elements and possible migration of bar or dune forms recorded as the oblique reflectors. The second phase is characterized by subparallel/sinuous reflectors (Fig. 2.b) and silt deposits (Fig. 3.c), indicating a more passive fill due to severe flow reduction (Aslan, 2013) -which in this case is due to the dam implementation in 1978. Dépret et al. (2019) also found that water level lowering following bypassing in the Rhône River resulted in a rapid dewatering process, which is confirmed here by the sharp increase in organic carbon content in this layer (Fig. 4.c). This depositional environment is therefore a hybrid of an active and passive channel fill, strongly influenced by river engineering. This interpretation was essential to identify the grain-size change as a date-marker that contributes to the robust dating of core PDR-1806. Additionally, it is worth noticing that its intermittent connection to the main channel might have resulted in a discontinuous sediment record.

Finally, the floodplain environment described in this study could be defined as a floodbasin: the lowest lying parts of a floodplain that act as a stilling basin in which suspended fines can settle from overbank flows after the coarser suspended debris have been deposited on levees (Aslan, 2013; Allen, 1965). Sediments from the floodplain environment in our study area are indeed fine (Fig. 3.d) and the absence of reflectors in the upper layer on the corresponding GPR profile (Fig. 2.c) is an indication of a

617 decantation process, resulting in a homogeneous sedimentary architecture with no tangible reflector.
618 In our case, the screening of coarser materials has been emphasized by the implementation of in-
619 channel infrastructures (Vauclin et al., 2019). Floodbasins often exhibit a network of small channels
620 (Allen, 1965), which used to be the case in the studied area, as proven by the two paleochannels clearly
621 identifiable on GPR10 (Fig. 2.c). Those filled channels are not discernible on the field nor recorded in
622 the historical maps, likely due to their small size: this demonstrates the interest of using GPR or another
623 geophysical method to understand the sedimentary context of a sediment core.

624 ### 4.3. Influence of depositional environments on sediment archives

625 When studying a sedimentary archive, one is ideally looking for a compromise between a good
626 temporal resolution and a long-term record, in an environment as preserved as possible. Those
627 features depend strongly on the depositional environment and are influenced by natural and
628 anthropogenic disturbances. As a consequence, finding a good sampling site for a sediment core is
629 rarely straightforward and requires investigation and/or a good knowledge of the study area.

630 Floodbasins have often been used as archives of historic contamination as they are less prone to
631 reworking than channel deposits and thus constitute long-term records of fine-grained sediments that
632 efficiently retain contaminants (Matys Grygar et al., 2016). The counterpart is that the record is most
633 likely intermittent, sediments being deposited in high-discharge conditions only. An estimation of the
634 overflow frequency is therefore essential for the interpretation of sedimentary sequences from such
635 an environment. In aggrading or corseted systems, the floodplain might not be actively flooded
636 anymore, meaning that even sediments close to the surface could be a few decades old. In our case,
637 the floodplain has been entirely disconnected from the channel since the late 1970s, and interpreting
638 the pollution trend from core PDR-C10a (Fig. 4.d) as the whole contamination chronicle would have
639 led to a wrong estimation of the pollution levels and dynamics in the area. Lewin and Macklin (2003)
640 noted that channel stability may cause overbank sedimentation to become self-limiting as the
641 floodplain aggrades and progressively becomes too elevated to be overflowed, and therefore reduces

642 over time the preservation potential of the floodplain environment. This is consistent with our
643 observations following the river training infrastructures implementation: the decline in floodplain-
644 channel connectivity was first translated into the deposition of finer-grained legacy sediments (Vauclin
645 et al., 2019), and was later exacerbated by the severe flow reduction associated with the dam
646 construction. River engineering therefore caused the loss of a recording environment, but it should
647 also be noted that the river training infrastructures stopped lateral channels migration, facilitating
648 sediment deposition without major reworking in the margins for several decades. Despite the recent
649 hiatus, the floodplain in our study still displays the longest sediment record (~1840s-1970s, cf. Fig. 6),
650 and therefore remains an essential sedimentary archive when properly interpreted.

651 Abandoned or partly disconnected channels are often considered as a good alternative to floodplains
652 to study recent river history (Bábek et al., 2008, Van Metre et al., 2008; Van Metre et al., 2015; Mourier
653 et al., 2014) as they are usually characterized by a reasonably good preservation potential and a better
654 stratigraphic resolution and continuity than floodplains due to their higher connectivity with the main
655 channel. The two secondary channels we studied showed similar recording tendencies but were also
656 influenced by the respective timings and dynamics of their disconnection. The temporal extent of the
657 archive is related to the date of the disconnection: the secondary channel that was partly disconnected
658 from the 1880s onward recorded a longer chronicle (1930s-2018) than the other channel (1960s-2018)
659 whose partial disconnection is mainly related to the bypass implementation in the 1970s. This
660 illustrates again the influence of human-induced river modification on the recording ability of the
661 various depositional environments. Additionally, the temporal resolution of the archive is linked to the
662 connection frequency of the channel environment (Fig. 6): the Ilon channel which is connected most
663 of the year has an accumulation rate more than twice as high (~3.2 cm.year^{-1}) as the Limony channel
664 (~1.3 cm.year^{-1}) that is only connected under high discharge conditions. Finally, the nature of the
665 channel fill influences the continuity and reliability of the archive: a passive fill such as in top parts of
666 the secondary channel cores ensures a deposition without reworking and therefore an archive without

667 significant hiatus, while an active channel fill -such as in the bottom half of core PDR-1806- is more
668 subject to sediment remobilization and errors in the archive interpretation.

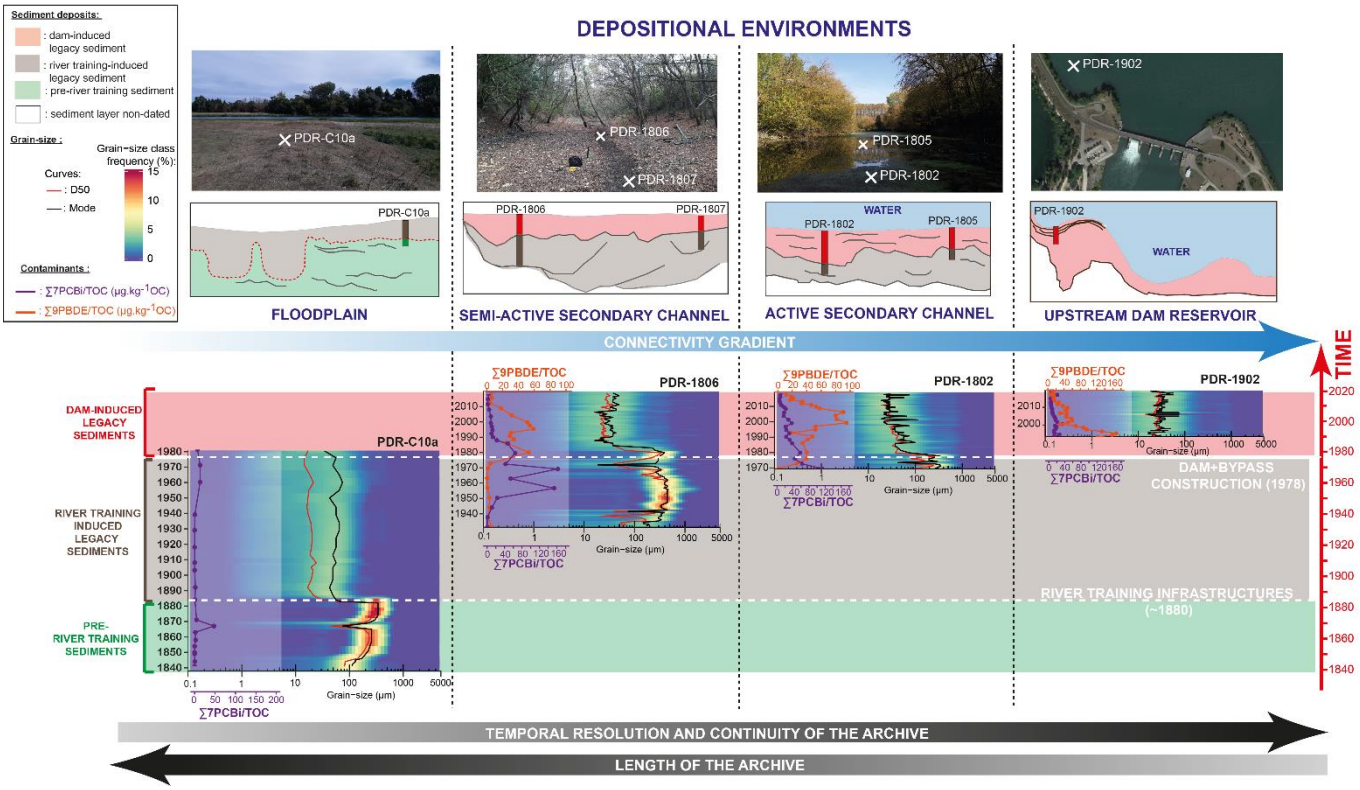

669

670 *Figure 6: A summary of the influence of depositional environments on sedimentary records: contamination trends and grain-*
671 *size events recorded depending on the environment (from left to right: floodplain, semi-active secondary channel, active*
672 *secondary channel and upstream dam reservoir).* [IN COLOR]

673 A fully anthropogenic depositional environment such as the run-of-river dam reservoir in this study
674 presents the highest temporal resolution and continuity, allowing to reliably discern subtle grain-size
675 and contamination variations. It is however temporally limited to the date of construction of the
676 infrastructure and might pose more practical challenges for the retrieving of sediment cores because
677 such environments tend to accumulate large amounts of sediments due to their proximity to the main
678 stream. Indeed, we did not manage to secure a core longer than ~1m although we know from the
679 bathymetric measurements that more than 5 m of sediments were stored in our sampling location.

680 Overall, each of the four depositional environments investigated in this study present strengths and
681 weaknesses as potential sediment archives. It is highly unlikely to come across a depositional

environment in a fluvial system that satisfies all the requirements of an ideal sedimentary archive: long-term record, good temporal resolution and continuity (i.e. absence of hiatuses). However, it is possible to reconstruct a composite archive by correlating several dated sedimentary sequences sampled in different deposition environments in a common study area, as illustrated in Fig. 6. While demanding, this methodology provides a robust archive that accounts for the spatial and temporal variability of the preservation potential of recent alluvial sediments. This is especially relevant when trying to understand the evolution of a complex and highly anthropized fluvial system such as the Rhône River, as river engineering tends to strongly modify the functioning of existing depositional environments (floodplain, secondary channels) and create new ones (reservoir), making the interpretation of sediment sequences even more challenging.

5. Conclusion

This work demonstrates the strong influence of the type of depositional environment on the sediment archive potential in a fluvial context. Indeed, the comparative and multi-compartments approach implemented in this study proved that the four studied environments recorded four different time-periods, and therefore different hydromorphological events and contamination trends. The different archives also show various degrees of continuity and temporal resolution that can only be inferred from a thorough understanding of the depositional environment and its functioning. For this purpose, the combination of geophysical surveys with sediment core following a rigorous sampling design is optimal, and we believe that such combination should be applied more frequently when investigating sediment deposits in actively shifting or adjusting river corridors. This is especially true in highly anthropized hydrosystems, as we proved that river engineering modified the recording potential of all four studied environments. The characteristics of a depositional environment can also provide invaluable information to elaborate or specify age-depth models of sedimentary archives, a task that can otherwise prove challenging in a fluvial context, especially with contemporary cores where conventional date-markers (^{137}Cs activity peaks, historical contaminants trends) might not be

707 recorded. In a context of growing environmental concerns regarding hydrosystems, a better
708 understanding of the impact of depositional environments on the recording potential of fluvial
709 sediment is essential. It may allow to correctly identify areas with a higher contamination and/or
710 remobilisation risk, but also to assess filling dynamics and the prospective need for restoration or
711 maintenance work such as dredging. It is an indispensable tool for current and future monitoring of
712 complex river systems that are continually evolving in association with anthropogenic activities.

713 Reference list

714 Abbasi, G., Li, L., Breivik, K., 2019. Global Historical Stocks and Emissions of PBDEs. Environ. Sci.
715 Technol. 53, 6330–6340. https://doi.org/10.1021/acs.est.8b07032

716 Allen, J.R.L., 1965. A Review of the Origin and Characteristics of Recent Alluvial Sediments.
717 Sedimentology 5, 89–191. https://doi.org/10.1111/j.1365-3091.1965.tb01561.x

718 Annan, A.P., Davis, J.L., 1977. Ground penetrating radar for high resolution mapping of soil and rock
719 stratigraphy 63–65.

720 Arnaud, F., Piégay, H., Schmitt, L., Rollet, A.J., Ferrier, V., Béal, D., 2015. Historical geomorphic
721 analysis (1932–2011) of a by-passed river reach in process-based restoration perspectives: The
722 Old Rhine downstream of the Kembs diversion dam (France, Germany). Geomorphology 236,
723 163–177. https://doi.org/10.1016/j.geomorph.2015.02.009

724 Arnaud-Fassetta, G., 2003. River channel changes in the Rhone Delta (France) since the end of the
725 Little Ice Age: geomorphological adjustment to hydroclimatic change and natural resource
726 management. CATENA 51, 141–172. https://doi.org/10.1016/S0341-8162(02)00093-0

727 Aslan, A., 2013. FLUVIAL ENVIRONMENTS | Sediments, in: Elias, S.A., Mock, C.J. (Eds.), Encyclopedia
728 of Quaternary Science (Second Edition). Elsevier, Amsterdam, pp. 663–675.
729 https://doi.org/10.1016/B978-0-444-53643-3.00111-4

730 Bábek, O., Hilscherová, K., Nehyba, S., Zeman, J., Famera, M., Francu, J., Holoubek, I., MacHát, J.,
731 Klánová, J., 2008. Contamination history of suspended river sediments accumulated in oxbow
732 lakes over the last 25 years: Morava River (Danube catchment area), Czech Republic. Journal of
733 Soils and Sediments 8, 165–176. https://doi.org/10.1007/s11368-008-0002-8

734 Baskaran, M., Nix, J., Kuyper, C., Karunakara, N., 2014. Problems with the dating of sediment core
735 using excess 210Pb in a freshwater system impacted by large scale watershed changes. Journal
736 of Environmental Radioactivity 138, 355–363. https://doi.org/10.1016/j.jenvrad.2014.07.006

737 Beres, M., Huggenberger, P., Green, A.G., Horstmeyer, H., 1999. Using two- and three-dimensional
738 georadar methods to characterize glaciofluvial architecture. Sedimentary Geology 129, 1–24.
739 https://doi.org/10.1016/S0037-0738(99)00053-6

740 Berger, J.-F., Shennan, S., Woodbridge, J., Palmisano, A., Mazier, F., Nuninger, L., Guillon, S., Doyen,
741 E., Begeot, C., Andrieu-Ponel, V., Azuara, J., Bevan, A., Fyfe, R., Roberts, C.N., 2019. Holocene
742 land cover and population dynamics in Southern France. The Holocene 29, 776–798.
743 https://doi.org/10.1177/0959683619826698

744 Bigus, P., Tobiszewski, M., Namieśnik, J., 2014. Historical records of organic pollutants in sediment
745 cores. Marine Pollution Bulletin 78, 26–42. https://doi.org/10.1016/j.marpolbul.2013.11.008

746 Blaauw, M., 2010. Methods and code for 'classical' age-modelling of radiocarbon sequences.
747 Quaternary Geochronology 5, 512–518. https://doi.org/10.1016/j.quageo.2010.01.002

748 Blott, S.J., Pye, K., 2001. GRADISTAT: a grain size distribution and statistics package for the analysis of
749 unconsolidated sediments. Earth Surface Processes and Landforms 26, 1237–1248.
750 https://doi.org/10.1002/esp.261

751 Bravard, J.-P., Landon, N., Peiry, J.-L., Piégay, H., 1999. Principles of engineering geomorphology for
752 managing channel erosion and bedload transport, examples from French rivers.
753 Geomorphology 31, 291–311. https://doi.org/10.1016/S0169-555X(99)00091-4

754 Breivik, K., Sweetman, A., Pacyna, J.M., Jones, K.C., 2002a. Towards a global historical emission
755 inventory for selected PCB congeners — a mass balance approach: 1. Global production and
756 consumption. Science of The Total Environment 290, 181–198. https://doi.org/10.1016/S0048-
757 9697(01)01075-0

758 Breivik, K., Sweetman, A., Pacyna, J.M., Jones, K.C., 2002b. Towards a global historical emission
759 inventory for selected PCB congeners — a mass balance approach: 2. Emissions. Science of The
760 Total Environment 290, 199–224. https://doi.org/10.1016/S0048-9697(01)01076-2

761 Brooks, A.P., Brierley, G.J., 1997. Geomorphic responses of lower Bega River to catchment
762 disturbance, 1851–1926. Geomorphology 18, 291–304. https://doi.org/10.1016/S0169-
763 555X(96)00033-5

764 Bruel, R., Sabatier, P., 2020. serac: a R package for ShortlivEd RAdionuclide Chronology of recent
765 sediment cores (preprint). EarthArXiv. https://doi.org/10.31223/osf.io/f4yma

766 Davis, J.L., Annan, A.P., 1989. Ground-Penetrating Radar for High-Resolution Mapping of Soil and
767 Rock Stratigraphy1. Geophysical Prospecting 37, 531–551. https://doi.org/10.1111/j.1365-
768 2478.1989.tb02221.x

769 Dépret, T., Riquier, J., Piégay, H., 2017. Evolution of abandoned channels: Insights on controlling
770 factors in a multi-pressure river system. Geomorphology 294, 99–118.
771 https://doi.org/10.1016/j.geomorph.2017.01.036

772 Desmet, M., Mourier, B., Mahler, B.J., Van Metre, P.C., Roux, G., Persat, H., Lefèvre, I., Peretti, A.,
773 Chapron, E., Simonneau, A., Miège, C., Babut, M., 2012. Spatial and temporal trends in PCBs in
774 sediment along the lower Rhône River, France. Science of The Total Environment 433, 189–197.
775 https://doi.org/10.1016/j.scitotenv.2012.06.044

776 Dhivert, E., Grosbois, C., Rodrigues, S., Desmet, M., 2015. Influence of fluvial environments on
777 sediment archiving processes and temporal pollutant dynamics (Upper Loire River, France).

778 Science of The Total Environment 505, 121–136.
779 https://doi.org/10.1016/j.scitotenv.2014.09.082

780 Dietze, E., Hartmann, K., Diekmann, B., IJmker, J., Lehmkuhl, F., Opitz, S., Stauch, G., Wünnemann, B.,
781 Borchers, A., 2012. An end-member algorithm for deciphering modern detrital processes from
782 lake sediments of Lake Donggi Cona, NE Tibetan Plateau, China. Sedimentary Geology 243, 169–
783 180. https://doi.org/ 10.1016/j.sedgeo.2011.09.014

784 Dietze, M., Dietze, E., Lomax, J., Fuchs, M., Kleber, A., Wells, S.G., 2016. Environmental history
785 recorded in aeolian deposits under stone pavements, Mojave Desert, USA. Quaternary
786 Research 85, 4–16. https://doi.org/10.1016/j.yqres.2015.11.007

787 Dotterweich, M., 2005. High-resolution reconstruction of a 1300-year-old gully system in northern
788 Bavaria, Germany: a basis for modelling long-term human-induced landscape evolution. The
789 Holocene 15, 994–1005. https://doi.org/10.1191/0959683605hl873ra

790 Eschbach, D., Schmitt, L., Imfeld, G., May, J.-H., Payraudeau, S., Preusser, F., Trauerstein, M.,
791 Skupinski, G., 2018. Long-term temporal trajectories to enhance restoration efficiency and
792 sustainability on large rivers: an interdisciplinary study. Hydrol. Earth Syst. Sci. 22, 2717–2737.
793 https://doi.org/10.5194/hess-22-2717-2018

794 Fuller, I.C., Macklin, M.G., Richardson, J.M., 2015. The Geography of the Anthropocene in New
795 Zealand: Differential River Catchment Response to Human Impact. Geographical Research 53,
796 255–269. https://doi.org/10.1111/1745-5871.12121

797 Goslar, T., Knaap, W.O. van der, Hicks, S., Andrič, M., Czernik, J., Goslar, E., Räsänen, S., Hyötylä, H.,
798 2005. Radiocarbon Dating of Modern Peat Profiles: Pre- and Post-Bomb 14C Variations in the
799 Construction of Age-Depth Models. Radiocarbon 47, 115–134.
800 https://doi.org/10.1017/S0033822200052243

GRAIE (Groupe de Recherche Rhône-Alpes, sur les Infrastructures et l'Eau), 2016. RhônEco : Le suivi scientifique de la restauration hydraulique et écologique du Rhône 2000-2015. Lyon.

Guédron, S., Amouroux, D., Sabatier, P., Desplanque, C., Develle, A.-L., Barre, J., Feng, C., Guiter, F., Arnaud, F., Reyss, J.L., Charlet, L., 2016. A hundred year record of industrial and urban development in French Alps combining Hg accumulation rates and isotope composition in sediment archives from Lake Luitel. Chemical Geology 431, 10–19. https://doi.org/10.1016/j.chemgeo.2016.03.016

Guzzella, L., Roscioli, C., Binelli, A., 2008. Contamination by polybrominated diphenyl ethers of sediments from the Lake Maggiore basin (Italy and Switzerland). Chemosphere 73, 1684–1691. https://doi.org/10.1016/j.chemosphere.2008.06.073

Huggenberger, P., Meier, E., Pugin, A., 1994. Ground-probing radar as a tool for heterogeneity estimation in gravel deposits: advances in data-processing and facies analysis. Journal of Applied Geophysics, Geophysics and Environment 31, 171–184. https://doi.org/10.1016/0926-9851(94)90056-6

James, L.A., 2013. Legacy sediment: Definitions and processes of episodically produced anthropogenic sediment. Anthropocene 2, 16–26. https://doi.org/10.1016/j.ancene.2013.04.001

Jol, H.M., 1995. Ground penetrating radar antennae frequencies and transmitter powers compared for penetration depth, resolution and reflection continuity1. Geophysical Prospecting 43, 693–709. https://doi.org/10.1111/j.1365-2478.1995.tb00275.x

Jones, A.F., Macklin, M.G., Brewer, P.A., 2012. A geochemical record of flooding on the upper River Severn, UK, during the last 3750 years. Geomorphology 179, 89–105. https://doi.org/10.1016/j.geomorph.2012.08.003

824 Karickhoff, S.W., Brown, D.S., Scott, T.A., 1979. Sorption of hydrophobic pollutants on natural
825 sediments. Water Research 13, 241–248. https://doi.org/10.1016/0043-1354(79)90201-X

826 Keeling, C.D., 1979. The Suess effect: 13Carbon-14Carbon interrelations. Environment International
827 2, 229–300. https://doi.org/10.1016/0160-4120(79)90005-9

828 Kohler, M., Zennegg, M., Bogdal, C., Gerecke, A.C., Schmid, P., V. Heeb, N., Sturm, M., Vonmont, H.,
829 E. Kohler, H.-P., Giger, W., 2008. Temporal Trends, Congener Patterns, and Sources of Octa-,
830 Nona-, and Decabromodiphenyl Ethers (PBDE) and Hexabromocyclododecanes (HBCD) in Swiss
831 Lake Sediments. Environ. Sci. Technol. 42, 6378–6384. https://doi.org/10.1021/es702586r

832 Krishnaswamy, S., Lal, D., Martin, J.M., Meybeck, M., 1971. Geochronology of lake sediments. Earth
833 and Planetary Science Letters 11, 407–414. https://doi.org/10.1016/0012-821X(71)90202-0

834 Lauzent, M., 2017. Etude de l'écodynamique des polluants organiques persistants et des
835 micropolluants halogénés d'intérêt émergent dans les milieux aquatiques (Chimie analytique).
836 Université de Bordeaux.

837 Lewin, J., Macklin, M.G., 2003. Preservation potential for Late Quaternary river alluvium. Journal of
838 Quaternary Science 18, 107–120. https://doi.org/10.1002/jqs.738

839 Liber, Y., Mourier, B., Marchand, P., Bichon, E., Perrodin, Y., Bedell, J.-P., 2019. Past and recent state
840 of sediment contamination by persistent organic pollutants (POPs) in the Rhône River:
841 Overview of ecotoxicological implications. Science of The Total Environment 646, 1037–1046.
842 https://doi.org/10.1016/j.scitotenv.2018.07.340

843 Lin, Y.-T., Schuettpelz, C.C., Wu, C.H., Fratta, D., 2009. A combined acoustic and electromagnetic
844 wave-based techniques for bathymetry and subbottom profiling in shallow waters. Journal of
845 Applied Geophysics 68, 203–218. https://doi.org/10.1016/j.jappgeo.2008.11.010

846 Lorgeoux, C., Moilleron, R., Gasperi, J., Ayrault, S., Bonté, P., Lefèvre, I., Tassin, B., 2016. Temporal
847 trends of persistent organic pollutants in dated sediment cores: Chemical fingerprinting of the

anthropogenic impacts in the Seine River basin, Paris. Science of The Total Environment 541, 1355–1363. https://doi.org/10.1016/j.scitotenv.2015.09.147

Malina, N., Mazlova, E.A., 2017. Temporal and spatial variation of polychlorinated biphenyls (PCBs) contamination in environmental compartments of highly polluted area in Central Russia. Chemosphere 185, 227–236. https://doi.org/10.1016/j.chemosphere.2017.06.137

Matys Grygar, T., Elznicová, J., Kiss, T., Smith, H.G., 2016. Using sedimentary archives to reconstruct pollution history and sediment provenance: The Ohře River, Czech Republic. CATENA 144, 109–129. https://doi.org/10.1016/j.catena.2016.05.004

Mourier, B., Desmet, M., Van Metre, P.C., Mahler, B.J., Perrodin, Y., Roux, G., Bedell, J.-P., Lefèvre, I., Babut, M., 2014. Historical records, sources, and spatial trends of PCBs along the Rhône River (France). Science of The Total Environment 476, 568–576. https://doi.org/10.1016/j.scitotenv.2014.01.026

Muir, D.C.G., Rose, N.L., 2007. Persistent Organic Pollutants in the Sediments of Lochnagar, in: Rose, N.L. (Ed.), Lochnagar: The Natural History of a Mountain Lake, Developments in Paleoenvironmental Research. Springer Netherlands, Dordrecht, pp. 375–402. https://doi.org/10.1007/1-4020-3986-7_16

Notebaert, B., Houbrechts, G., Verstraeten, G., Broothaerts, N., Haeckx, J., Reynders, M., Govers, G., Petit, F., Poesen, J., 2011. Fluvial architecture of Belgian river systems in contrasting environments: implications for reconstructing the sedimentation history. Netherlands Journal of Geosciences - Geologie en Mijnbouw 90.

Nylund, K., Asplund, L., Jansson, B., Jonsson, P., Litzén, K., Sellström, U., 1992. Analysis of some polyhalogenated organic pollutants in sediment and sewage sludge. Chemosphere 24, 1721–1730. https://doi.org/10.1016/0045-6535(92)90227-I

871 Parrot, E., 2015. Analyse spatio-temporelle de la morphologie du chenal du Rhône du Léman à la
872 Méditerranée (thesis). Lyon 3.

873 Petit, F., Poinsart, D., Bravard, J.-P., 1996. Channel incision, gravel mining and bedload transport in
874 the Rhône river upstream of Lyon, France ("canal de Miribel"). CATENA 26, 209–226.
875 https://doi.org/10.1016/0341-8162(95)00047-X

876 Pouzet, P., Maanan, M., 2020. Temporal approaches of historical extreme storm events based on
877 sedimentological archives. Journal of African Earth Sciences 162, 103710.
878 https://doi.org/10.1016/j.jafrearsci.2019.103710

879 Ritchie, J.C., McHenry, J.R., 1990. Application of Radioactive Fallout Cesium-137 for Measuring Soil
880 Erosion and Sediment Accumulation Rates and Patterns: A Review. Journal of Environment
881 Quality 19, 215–233. https://doi.org/10.2134/jeq1990.00472425001900020006x

882 Simonneau, A., Doyen, E., Chapron, E., Millet, L., Vannière, B., Di Giovanni, C., Bossard, N., Tachikawa,
883 K., Bard, E., Albéric, P., Desmet, M., Roux, G., Lajeunesse, P., Berger, J.F., Arnaud, F., 2013.
884 Holocene land-use evolution and associated soil erosion in the French Prealps inferred from
885 Lake Paladru sediments and archaeological evidences. Journal of Archaeological Science 40,
886 1636–1645. https://doi.org/10.1016/j.jas.2012.12.002

887 Słowik, M., 2015. Is history of rivers important in restoration projects? The example of human impact
888 on a lowland river valley (the Obra River, Poland). Geomorphology 251, 50–63.
889 https://doi.org/10.1016/j.geomorph.2015.05.031

890 Surian, N., Rinaldi, M., 2003. Morphological response to river engineering and management in
891 alluvial channels in Italy. Geomorphology 50, 307–326. https://doi.org/10.1016/S0169-
892 555X(02)00219-2

893 Tena, A., Piégay, H., Seignemartin, G., Barra, A., Berger, J.F., Mourier, B., Winiarski, T., 2020.
894 Cumulative effects of channel correction and regulation on floodplain terrestrialisation patterns
895 and connectivity. Geomorphology 107034. https://doi.org/10.1016/j.geomorph.2020.107034

896 Toonen, W.H.J., Winkels, T.G., Cohen, K.M., Prins, M.A., Middelkoop, H., 2015. Lower Rhine historical
897 flood magnitudes of the last 450years reproduced from grain-size measurements of flood
898 deposits using End Member Modelling. CATENA 130, 69–81.
899 https://doi.org/10.1016/j.catena.2014.12.004

900 Van Metre, P.C., Babut, M., Mourier, B., Mahler, B.J., Roux, G., Desmet, M., 2015. Declining Dioxin
901 Concentrations in the Rhone River Basin, France, Attest to the Effectiveness of Emissions
902 Controls. Environ. Sci. Technol. 49, 12723–12730. https://doi.org/10.1021/acs.est.5b03416

903 Van Metre, P.C., Mesnage, V., Laignel, B., Motelay, A., Deloffre, J., 2008. Origins of Sediment-
904 Associated Contaminants to the Marais Vernier, the Seine Estuary, France. Water Air Soil Pollut
905 191, 331–344. https://doi.org/10.1007/s11270-008-9628-9

906 Vanwalleghem, T., Bork, H.R., Poesen, J., Dotterweich, M., Schmidtchen, G., Deckers, J., Scheers, S.,
907 Martens, M., 2006. Prehistoric and Roman gullying in the European loess belt: a case study from
908 central Belgium. The Holocene 16, 393–401. https://doi.org/10.1191/0959683606hl935rp

909 Vauclin, S., Mourier, B., Piégay, H., Winiarski, T., 2020. Legacy sediments in a European context: The
910 example of infrastructure-induced sediments on the Rhône River. Anthropocene 31, 100248.
911 https://doi.org/10.1016/j.ancene.2020.100248

912 Vauclin, S., Mourier, B., Tena, A., Piégay, H., Winiarski, T., 2019. Effects of river infrastructures on the
913 floodplain sedimentary environment in the Rhône River. J Soils Sediments 20, 2697–2708.
914 https://doi.org/10.1007/s11368-019-02449-6

915 Vénisseau, A., Bichon, E., Lesquin, E., Guiffard, I., Marchand, P., Le Bizec, B., 2015. Simultaneous
916 Analysis of PBDEs, PBBS, HBCDDs, TBBPA and Additional Flame Retardants in Food. Presented at
917 the 7th International Symposium on Flame Retardants (BFR), Beijing, China.

918 Vliet-Lanoë, B.V., Goslin, J., Hallégouët, B., Hénaff, A., Delacourt, C., Fernane, A., Franzetti, M.,
919 Cornec, E.L., Roy, P.L., Penaud, A., 2014. Middle- to late-Holocene storminess in Brittany (NW
920 France): Part I – morphological impact and stratigraphical record: The Holocene.
921 https://doi.org/10.1177/0959683613519687

922 Walter, R.C., Merritts, D.J., 2008. Natural Streams and the Legacy of Water-Powered Mills. Science
923 319, 299–304. https://doi.org/10.1126/science.1151716

924 Wania, F., 1999. Global Modelling of Polychlorinated Biphenyls. WECC Wania Environmental
925 Chemists Corp. 22.

926 Weltje, G.J., Prins, M.A., 2007. Genetically meaningful decomposition of grain-size distributions.
927 Sedimentary Geology 202, 409–424. https://doi.org/10.1016/j.sedgeo.2007.03.007

928 Weltje, G.J., Prins, M.A., 2003. Muddled or mixed? Inferring paleoclimate from size distributions of
929 deep-sea clastics. Sediment Geol, SEDIMENT GEOL, Sedimentary Geology 162, 39–62.
930 https://doi.org/10.1016/S0037-0738(03)00235-5

931 Wohl, E., 2015. Legacy effects on sediments in river corridors. Earth-Science Reviews 147, 30–53.
932 https://doi.org/10.1016/j.earscirev.2015.05.001

933 Wohl, E., Angermeier, P.L., Bledsoe, B., Kondolf, G.M., MacDonnell, L., Merritt, D.M., Palmer, M.A.,
934 Poff, N.L., Tarboton, D., 2005. River restoration. Water Resources Research 41.
935 https://doi.org/10.1029/2005WR003985

936 Zegers, B.N., Lewis, W.E., Booij, K., Smittenberg, R.H., Boer, W., de Boer, J., Boon, J.P., 2003. Levels of
937 Polybrominated Diphenyl Ether Flame Retardants in Sediment Cores from Western Europe.
938 Environ. Sci. Technol. 37, 3803–3807. https://doi.org/10.1021/es034226o

939 Zolitschka, B., Anselmetti, F., Ariztegui, D., Corbella, H., Francus, P., Lücke, A., Maidana, N.I.,
940 Ohlendorf, C., Schäbitz, F., Wastegård, S., 2013. Environment and climate of the last
941 51,000 years – new insights from the Potrok Aike maar lake Sediment Archive Drilling prOject
942 (PASADO). Quaternary Science Reviews 71, 1–12.
943 https://doi.org/10.1016/j.quascirev.2012.11.024

944